Enhanced ion acceleration due to high-shear tangential discontinuities upstream of quasi-perpendicular shocks

K. Steinvall[1], **I. Gingell**[1]

[1]School of Physics and Astronomy, University of Southampton, Southampton SO17 1BJ, United Kingdom

Key Points:

- Bursts of energetic ions can appear upstream of quasi-perpendicular shocks due to highly sheared upstream tangential discontinuities
- The magnetic field change of the discontinuity enables the shock-reflected ions to be further energized by the convection electric field
- This process results in a local acceleration efficiency comparable to that of quasi-parallel shocks under steady upstream conditions

Corresponding author: Konrad Steinvall, l.k.g.steinvall@soton.ac.uk

Corresponding author: Imogen Gingell, i.l.gingell@soton.ac.uk

Abstract

Collisionless shock waves are efficient ion accelerators. Previous numerical and observational studies have shown that quasi-parallel ($Q_{\parallel}$) shocks are more effective than quasi-perpendicular ($Q_{\perp}$) shocks at generating energetic ions under steady upstream conditions. Here, we use a local, 2D, hybrid particle-in-cell model to investigate how ion acceleration at super-critical $Q_{\perp}$ shocks is modulated when tangential discontinuities (TDs) with large magnetic shear are present in the upstream plasma. We show that such TDs can significantly increase the ion acceleration efficiency of $Q_{\perp}$ shocks, up to a level comparable to $Q_{\parallel}$ shocks. Using data from the hybrid model and test particle simulations, we show that the enhanced energization is related to the magnetic field change associated with the discontinuity. When shock-reflected ions cross the TD during their upstream gyromotion, the sharp field change causes the ions to propagate further upstream, and gain additional energy from the convection electric field associated with the upstream plasma flow. Our findings illustrate that the presence of upstream discontinuities can lead to bursts of energetic ions, even when they do not trigger the formation of foreshock transients. These results emphasize the importance of time-variable upstream conditions when considering ion energization at shocks.

1 Introduction

Collisionless shock waves are found ubiquitously in space plasmas. Through processes such as diffusive shock acceleration (e.g. Drury, 1983; Blandford & Eichler, 1987) and shock drift acceleration (e.g. Pesses et al., 1982; Armstrong et al., 1985), shocks are able to accelerate ions and electrons to high energies. The question of particle acceleration at shocks has been studied extensively for a long time (e.g. Asbridge et al., 1968; Giacalone et al., 1992; Giacalone, 2003; Malkov & Drury, 2001; Masters et al., 2013; Chen et al., 2018). Recent observational and numerical studies have shown that the degree to which shocks partition energy to high-energy ions depends strongly on the angle, θ_{Bn}, between the shock normal and the upstream magnetic field (Caprioli & Spitkovsky, 2014; Johlander et al., 2021; Lalti et al., 2022). Ion acceleration is significantly more efficient in the quasi-parallel regime ($Q_{\parallel}$), where $\theta_{Bn} < 45°$, compared to the quasi-perpendicular ($Q_{\perp}$; $\theta_{Bn} > 45°$) regime, where ion energization is negligible in comparison. However, these previous studies have generally been limited to the case of steady upstream conditions, and their conclusions are therefore likely not representative of the general case

of dynamic upstream conditions. Indeed, foreshock transients such as hot flow anomalies and foreshock bubbles, which can be formed during the interaction of shocks with upstream discontinuities (Zhang et al., 2022, and references therein), have been found to produce increased fluxes of energetic ions (e.g. T. Z. Liu et al., 2018; Turner et al., 2018; Omidi et al., 2021), illustrating the significant effects dynamic upstream conditions can have. While foreshock transients are indeed effective ion accelerators, they are not always generated when discontinuities interact with the shock (e.g. Schwartz et al., 2000; T. Z. Liu et al., 2023). It is therefore of interest to investigate whether or not upstream discontinuities have an effect on ion acceleration even when they do not result in the formation of foreshock transients.

In the present study, we use hybrid particle-in-cell (PIC) and test particle simulations to investigate ion acceleration due to highly sheared upstream tangential discontinuities at super-critical $Q_\perp$ shocks. We show that such discontinuities can significantly enhance the production of energetic ions (i.e. ions with energy larger than 10 times the bulk inflow kinetic energy), without the formation of foreshock transients. The underlying acceleration mechanism is that the TDs modify the gyromotion of reflected ions in the upstream, enabling additional energization by the convection electric field.

2 Numerical setup

The local 2.5D hybrid code used here is the same as in Steinvall and Gingell (2024a). The code builds on the fusion of the full PIC code EPOCH (Arber et al., 2015) with the current advance method and cyclic leapfrog (CAM-CL) algorithm (Matthews, 1994), as presented by Gingell et al. (2023). In summary, ions (protons) are treated as particles, whereas electrons are described as a massless charge-neutralizing fluid. Space is resolved in two dimensions (x, y) on a $120d_{i0} \times 120d_{i0}$ grid, d_{i0} being the upstream ion inertial length, with a resolution of $\Delta x = \Delta y = 0.15d_{i0}$. Each grid cell is initialized with 100 macro particles per cell. The fields and momenta have 3 components, with $\partial/\partial z = 0$. The $x = 0$ boundary is open, and the time dependent upstream plasma is injected through it with a velocity v_0. Particles are specularly reflected at the $x = 120d_{i0}$ boundary, resulting in the formation of a shock propagating in the $-x$ direction. The simulation is therefore in the downstream plasma frame. The initial magnetic field is in the xy-plane for all runs. This, together with the fact that the shock surface is in the yz-plane, implies that θ_{Bn} determines the orientation of the TD, the surface of which is tangential

to the magnetic field lines. For this reason, we need to use open y-boundaries when $\theta_{Bn} \neq 90°$, and we can use periodic y-boundaries only when $\theta_{Bn} = 90°$. To avoid potential edge effects due to the open boundaries, we restrict our analysis to the y-range $(30, 90)d_{i0}$. The flow is initialized by applying an initial convection electric field $E_z = -v_0 B_{0y}$ over the whole domain.

We investigate the effect of two different TD models. (1) Force-free TDs, which, in the local coordinates of the TD (x', y', z') are of the form $B_{x'} = B_n$, $B_{y'} = B_t \cos(\theta(x'))$, $B_{z'} = B_t \sin(\theta(x'))$, where $B_n = 0$ and $B_t = B_0$ are the magnetic field components normal and tangential to the TD respectively, and $\theta(x') = [1 + \tanh(x'/L)]\,\Delta\varphi_B/2$, with L being the half-width and $\Delta\varphi_B$ the magnetic shear angle. Unless otherwise specified, we use a value of $\Delta\varphi_B = 180°$. (2) Harris TDs of the form $B_{x'} = B_n = 0$, $B_{y'} = B_0 \tanh(x'/L)$, $B_{z'} = 0$, with a corresponding density profile $n = n_0 + \delta n \,\mathrm{sech}^2(x'/L)$, where $\delta n = B_0^2/(2\mu_0 T_0)$, and T_0 is the ambient plasma temperature.

We choose shock and plasma parameters that are relevant for the Earth's bow shock. As such, we select an upstream plasma beta $\beta_0 = 1$ for both ions and electrons, inflow speeds $v_0 \in \{6, 9, 12\}v_{A0}$, where v_{A0} is the upstream Alfvén speed, yielding shocks with approximate Alfvénic Mach numbers $M_A \in \{8, 12, 15\}$, and $\theta_{Bn} \in \{70°, 80°, 90°\}$.

3 Results

3.1 Temporal evolution

We illustrate the evolution of the system for the case of a Harris TD of $L = 3d_{i0}$ interacting with a $\theta_{Bn} = 70°$, $M_A = 12$ shock in Fig. 1. There we plot, as black points, the locations of the ions that reach kinetic energies $\mathcal{E}$ larger than 10 times the upstream bulk kinetic energy $\mathcal{E}_0$ for the first time. We refer to ions satisfying $\mathcal{E} \geq 10\mathcal{E}_0$ as "energetic", in conformity with Johlander et al. (2021). At time $t\omega_{ci0} = 12.57$, before the TD arrives (Fig. 1a), a small number of ions are energized (i.e. reach the $10\mathcal{E}_0$ threshold) each time step. When the TD impacts the shock at $t\omega_{ci0} = 15.71$ (Fig. 1b), we observe an increase of energetic ions just downstream of the TD. In addition, energetic ions start appearing around $20d_{i0}$ upstream of the shock. Shortly after, at $t\omega_{ci0} = 18.22$ (Fig. 1c), there is a significant increase of energetic ions in the upstream. After a few more gyrotimes ω_{ci0}^{-1} (Fig. 1d), ions are no longer being energized in the upstream, and they are instead preferentially energized near the TD in the downstream. In the downstream, the

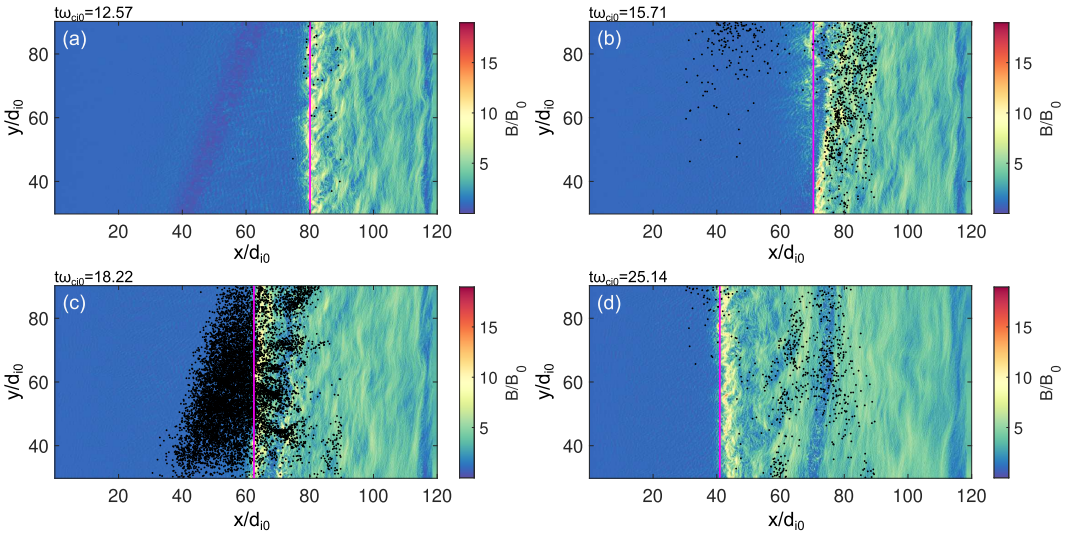

Figure 1. Snapshots of the shock-TD interaction at four different times for a Harris TD ($L = 3d_{i0}$, $\theta_{Bn} = 70^\circ$, $M_A = 12$). (a) Before the TD reaches the shock. (b) When the TD impinges on the shock. (c) After the TD has just propagated past the shock. (d) When the TD is far downstream of the shock. The black dots show the locations of individual ions that reach the energy threshold ($\mathcal{E} \geq 10\mathcal{E}_0$) for the first time. The magenta line indicates the shock location. The (Harris) TD can be identified as the tilted $|\mathbf{B}|$ depression, e.g. in the $x/d_{i0} = (40, 60)$ range in panel (a) and $x/d_{i0} = (70, 75)$ in panel (d).

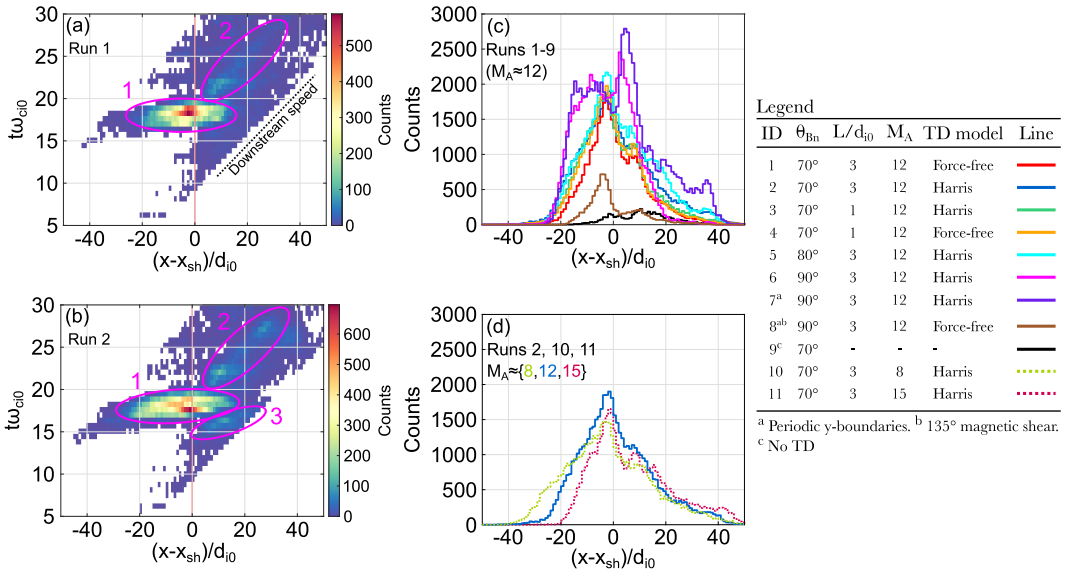

Figure 2. Histograms of energetic ions. (a) 2D histogram showing the position relative to the shock ($x_{\rm sh}(t)$ being the position of the shock) and time where ions reach $\mathcal{E} \geq 10\mathcal{E}_0$ for a force-free TD (run 1) (b) Same as (a), but for a Harris TD (run 2). (c) 1D histogram for all times, comparing the different $M_A = 12$ runs. (d) Same format as (c) for different M_A.

TD has undergone magnetic reconnection, resulting in the formation of magnetic islands. The evolution is qualitatively similar in all high-shear runs.

Depending on whether the TD is of the force-free or Harris type, we can distinguish 2 to 3 sources of energetic ions. These sources are identified in the $x-t$ histograms of the ion energization location in Fig. 2a for the force-free case, and Fig. 2b for the Harris case. In both cases, the upstream source (marked '1' in the figure) is the dominant source of energetic ions, as was indicated by Fig. 1c. Source 2 first appears downstream of the shock after the shock-TD collision, and moves downstream (in the shock frame) with the shocked plasma, continuing to energize ions for $\sim 10\omega_{ci0}^{-1}$. This corresponds to the energetic ions near the TD in Fig. 1d, and is likely a result of the dynamics driven by magnetic reconnection of the TD, which is triggered when the TD is compressed by the shock (Lin, 1997; Hamrin et al., 2019). Source 3, which only appears in the Harris case, propagates faster into the downstream than the plasma flow, and generates a small number of energetic ions. This is likely a magnetosonic perturbation that is launched when the Harris TD interacts with the shock. Such magnetosonic perturbations have been studied in detail by Nagata et al. (2008) and Maynard et al. (2007, 2008). The same sources

appear in all our simulation runs, and the number of energetic ions produced is not sensitive to θ_{Bn}, M_A, L, or TD type, as illustrated in Figs. 2c and 2d, where we present 1D histograms of the x-position where ions first reach the energy threshold, summing over all times. When we reduce the magnetic shear from 180° to 135° (brown histogram in Fig. 2c), the number of energetic ions is reduced to a factor ≈ 0.15 in the $\theta_{Bn} = 90°$ case. Further reducing the shear to 100° (not shown) reduces the energization to close to the no-TD level. From this we conclude that high-shear TDs are able to produce a significant number of energetic ions at $Q_\perp$ shocks, where, for the case of a uniform upstream, one would expect minimal ion energization. Because the upstream source is so dominant, it is this source that we will focus on and devote the remainder of this article to.

Before moving on, first a brief comment on the effects of the open y-boundaries. To ensure that our results are not influenced by the boundary conditions, we compare two $\theta_{Bn} = 90°$ runs with open (magneta) and periodic (purple) y-boundaries in Fig. 2c. The runs are in good agreement, particularly in our region of interest, namely the upstream. In the downstream, the difference in life-time of the ions (finite in the open case, infinite in the periodic case) leads to some differences in the number of accelerated ions. This comparison shows that the effects of the open boundaries are negligible for the upstream source.

3.2 Acceleration mechanism

Next, we turn to the question: what is the mechanism that accelerates the ions to high energies? To answer this question, we will focus our effort on the $\theta_{Bn} = 90°$ case with periodic y-boundaries (Run 7 in Fig. 2c), since this gives a simplifying symmetry with respect to y. In Fig. 3a-c we plot the time history of one ion which exceeds the energy threshold. This example is, as we will later see, representative of most ions that are energized upstream. The ion is reflected at the shock by the cross-shock electric field at $t\omega_{ci0} \approx 11$ (Fig. 3c), whereafter it starts gyrating in the upstream. During the upstream gyromotion, the ion is energized by the upstream convection electric field (Figs. 3b and 3d) to $5\mathcal{E}_0$. Before the ion has time to return to the shock, it crosses the TD (yellow shaded region), and the associated change of B_y reverses the gyromotion as shown in Fig. 3e, where the blue data correspond to values upstream of the shock, and the turning point at $v_x/v_0 \approx 0$, $v_z/v_0 \approx -2$ is due to the first TD crossing. The reversed gyromotion

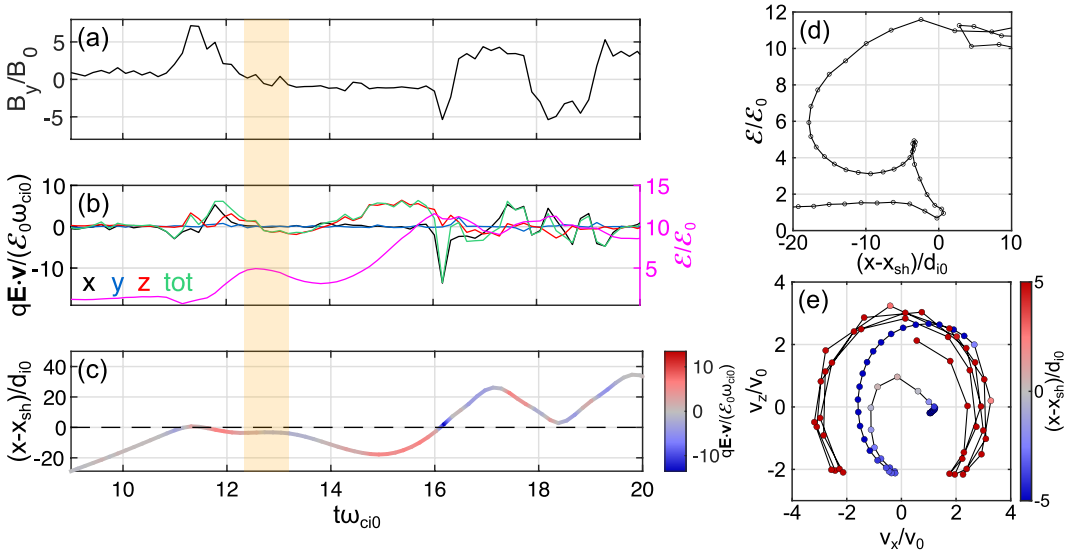

Figure 3. Energetic ion evolution in the hybrid model. (a) Magnetic field y-component as experienced by the ion in the lab frame as a function of time. (b) Left axis: work done on the ion by **E** decomposed into the three contributions (black, blue, red) and their sum (green). Right axis (magenta): energy of the ion. (c) Distance to the shock with the work done on the ion color-coded (i.e. green curve in (b)). The shaded region in (a-c) highlights TD crossing. (d) Ion energy vs. distance to shock. (e) Ion v_x-v_z phase space trajectory with distance to shock color-coded.

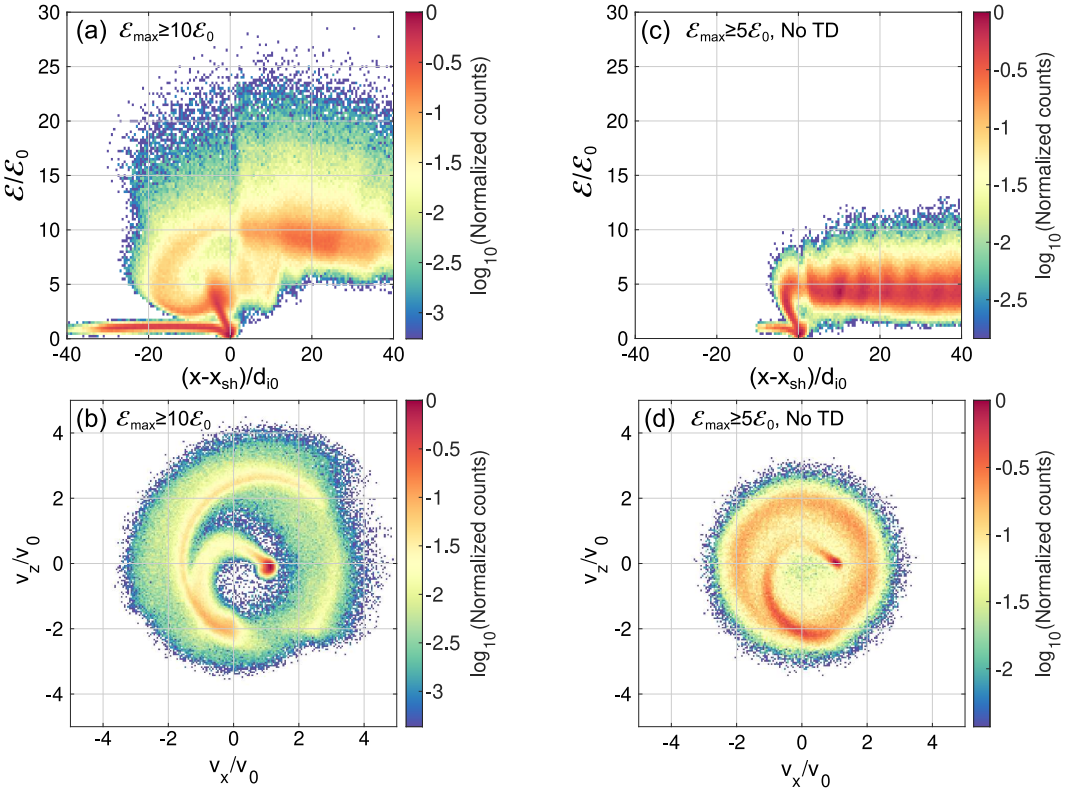

Figure 4. Statistics of x-$\mathcal{E}$ and v_x-v_z trajectories from the hybrid model. (a-b) Ions which satisfy $\mathcal{E}_{\max} \geq 10\mathcal{E}_0$ when the TD is near the shock and can influence the ion motion. (c-d) Ions which satisfy $\mathcal{E}_{\max} \geq 5\mathcal{E}_0$ when the TD is far upstream of the shock.

causes the ion to travel almost $20d_{i0}$ upstream (Figs. 3c and 3d), and enables further energization by the convection electric field. The ion reaches an energy close to $12\mathcal{E}_0$, before crossing the shock at $t\omega_{ci0} \approx 16$. After the crossing, the ion continues its meandering motion around the TD in the downstream for the remainder of the simulation, as seen by the red crescent trajectory in Fig. 3e.

To ensure that the mechanism described above is representative for the energetic ions, we compile 2D histograms of the x-$\mathcal{E}$ and v_x-v_z trajectories (corresponding to Fig. 3d and e) for the ions that eventually satisfy $\mathcal{E} \geq 10\mathcal{E}_0$. These are shown in Figs. 4a and 4b. The resulting histograms show that the most energized ions undergo the same kind of acceleration process as the ion shown in Fig. 3. We note that the energized ions tend to cross the TD near the $v_x = 0$ part of their gyromotion, corresponding to motion tangential to the shock surface. Repeating the same analysis on ions that reach the shock well before the TD, using a weaker threshold of $5\mathcal{E}_0$, yields the results in Figs. 4c and

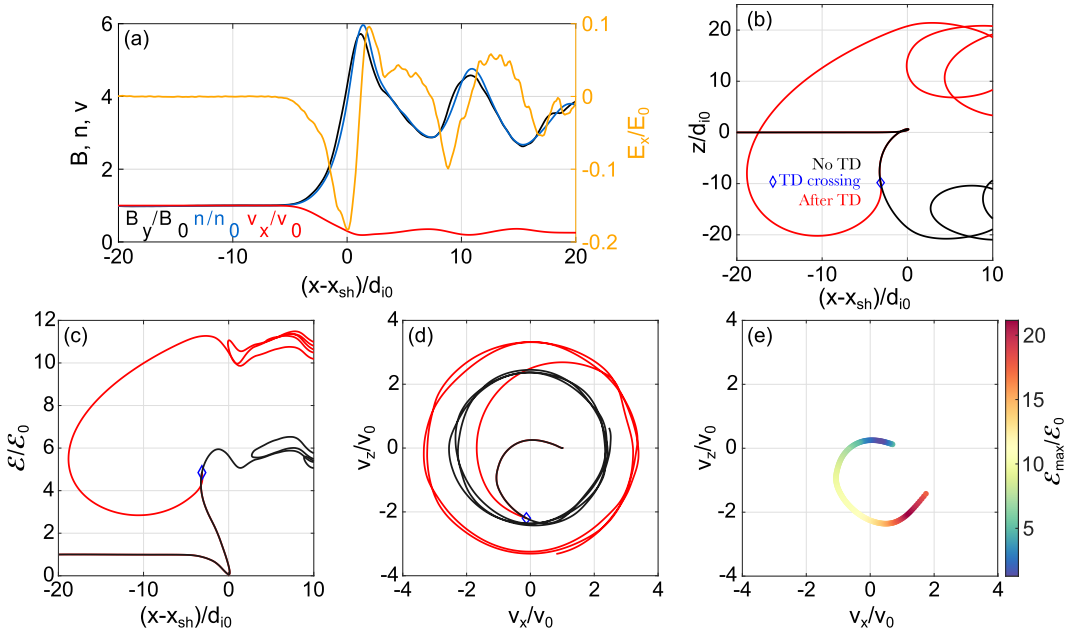

Figure 5. Test particle simulation results. (a) Magnetic field (black), density (blue), velocity (red), and corresponding electric field (orange) profile used in the test particle simulation. (b) Spatial trajectories of two ions with identical initial conditions, one of which crosses a TD (red), and one that does not (black). The blue diamond indicates when the red ion crosses the TD and the two curves diverge. (c,d) Energy versus position and velocity space trajectories for the ions in (b). (e) Color plot showing how the maximum energy of an ion depends on its gyrophase at the time it crosses the TD.

4d. Clearly, without the TD interaction, only a very small number of ions reach $10\mathcal{E}_0$, and they do so only in the downstream. We can thus conclude that the TD is necessary for accelerating the ions to high energies.

3.3 Test particle simulations

To test the proposed energization mechanism we preform a series of test particle simulations. We construct a 1D shock model based on the $B_y(x)$, $n(x)$, and $v_x(x)$ profiles from the hybrid model. To remove potential small scale effects, we average the profiles in y, and apply a moving average to smooth them further. We then compute the electric field components from Ohm's law, $E_x = -(en)^{-1}(J_z B_y + T_{e0}\partial n/\partial x)$, $E_z = -v_x B_y$, where $J_z = \mu_0^{-1}\partial B_y/\partial x$, and we have used an isothermal electron equation of state $p_e(x) = n(x)T_{e0}$. The different profiles are plotted in Fig 5a. For simplicity, we

perform the simulation in the shock-frame, and transform the results to the downstream frame. The TD crossing is modeled as an instantaneous change of the sign of $B_y(x)$ in the whole domain. This gives us the freedom to apply the TD crossing at an arbitrary time, and therefore also at an arbitrary gyrophase of the test ion. In Figs. 5b-d, we show the trajectories of two identical test particles in different parameter spaces. The black data correspond to a test particle that does not interact with a TD, whereas the red data correspond to a test particle that crosses the TD after reflection, at the position marked by the blue diamond. The data are in excellent agreement with the single ion presented in Fig. 3 and the statistical results of Fig. 4. We note, however, that in order for the ions to be reflected in the test particle simulation, we have had to increase E_x by a factor of around 10-15. Such an extra factor is needed because the cross-shock potential (and E-field) in the hybrid model is highly modulated along the shock surface, with peaks occasionally reaching amplitudes of more than 20 times the y-average. Ions are naturally preferentially reflected in these regions of high cross-shock potential. It should be noted that recent spacecraft observations indicate that the cross-shock potential at physical shocks might not be large-scale coherent structures as indicated by Fig. 5a, but rather the sum of many small-scale structures (Chen et al., 2018; Wilson et al., 2021). However, as we will later see, it is not the details of the reflection process that are important for the observed particle energization, but rather what happens after reflection.

In Fig. 5e, we investigate how the maximum energy $\mathcal{E}_{\max}$ changes depending on where the ion is in the v_x-v_z space during the TD crossing. The color at each point shows the value of $\mathcal{E}_{\max}$ obtained if the TD crossing occurs there. These results show that ions gain more energy the later they cross the TD. The $10\mathcal{E}_0$ threshold is reached when the ions have a small negative v_x and a large negative v_z, which is consistent with the crossing points of the ions in Fig. 2b. Moreover, Fig. 5e shows that the ions gain more energy the later they are in their gyrophase when crossing the TD, with a maximum of $\approx 20\mathcal{E}_0$ at $v_x/v_0 \approx 1$. In reality, however, when $v_x > 1$, the ions propagate away from the TD, and are therefore unable to cross it. We conclude that the simple test particle model can accurately reproduce the results of the hybrid model, showing that the main effect the TD has on ion acceleration is to reverse the gyro-motion, enabling increased energization by the convection electric field. This conclusion has the consequence that the functional shape of the discontinuity is not important, so long as its thickness is much smaller than the gyroradii of the reflected ions. Thus, the above mechanism should also occur

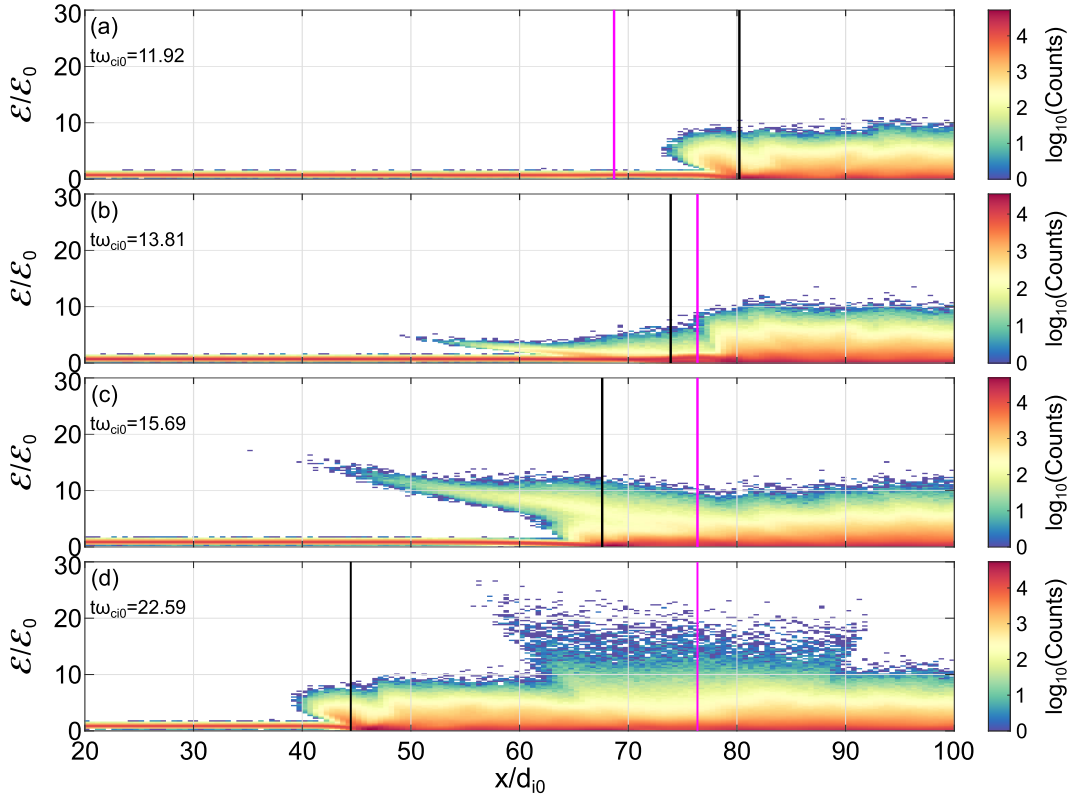

Figure 6. Ion energy spectrum as a function of x for four different times. (a) Before the TD reflected ions reach the TD. (b) Just after the reflected ions have crossed the TD. (c) When the meandering ions are energized by the convection E-field. (d) After the TD has propagated far downstream. The approximate shock and TD positions are shown with the black and magenta lines, respectively.

when the magnetic field change is due to, for example, narrow rotational discontinuities or more exotic structures such as switchback boundaries.

3.4 Downstream signatures

With the acceleration mechanism established, we finally investigate the spatial and temporal signatures of this process in Fig. 6. When the TD (as indicated with the magenta line) approaches the shock (Fig. 6b), the reflected ions that cross the TD form a localized band in energy-space, which reaches far upstream. These ions are then energized in the upstream (Fig. 6c) and eventually pass through the shock. In the downstream, the energized ions are observed as a significant local temperature enhancement near the TD (Fig. 6d). The results presented in Fig. 6d have implications for the analysis of in-

situ data. Since the TD is undergoing magnetic reconnection, reconnection signatures could be observed by a spacecraft crossing the TD. This, together with the locally heated plasma, may give the impression that the heating is due to reconnection. However, as we have shown in this study, the vast majority of these energetic ions were energized upstream of the shock. We therefore emphasize that caution needs to be exercised when using spacecraft data to analyze highly sheared TDs of solar wind origin in the magnetosheath.

Following Caprioli and Spitkovsky (2014), Johlander et al. (2021), and Lalti et al. (2022), we quantify the acceleration efficiency α in a (downstream) spatial interval as the fraction of energy carried by the $\mathcal{E} \geq 10\mathcal{E}_0$ ions. Before the TD arrives ($t\omega_{ci0} = 11.92$; Fig. 6a), we compute α in the $x \in [87, 97]d_{i0}$ interval, obtaining $\alpha = 0.03\%$, consistent with the expectation that $Q_\perp$ shocks have a very low acceleration efficiency. However, once the TD has propagated into the downstream ($t\omega_{ci0} = 22.59$; Fig. 6d), performing the same analysis in the $x \in [70, 80]d_{i0}$ interval gives $\alpha = 2\%$, which is comparable to that of $Q_\parallel$ shocks (Johlander et al., 2021). Taking a lower energy threshold of $5\mathcal{E}_0$ yields an acceleration efficiency of 9% without the TD, and 14% with the TD. These results show that highly sheared TDs are able to significantly increase the acceleration efficiency of $Q_\perp$ shocks in a wide region (around $\pm 15d_{i0}$) around the TD. Thus, even if no foreshock transients are formed, highly sheared TDs remain important sources of energetic ions at $Q_\perp$ shocks.

4 Summary and conclusions

In summary, we use a local 2.5D hybrid-PIC model and test particle simulations to investigate how highly sheared upstream tangential discontinuities influence the energization of ions at quasi-perpendicular shocks in the absence of foreshock transients. Our results (Fig. 2) show that there are three mechanisms through which TDs can generate energetic ions (defined in the downstream frame as ions with at least 10 times the upstream kinetic energy). Two mechanisms yield minor contributions, and they are: magnetic reconnection of the TDs after being compressed by the shock (Lin, 1997; Hamrin et al., 2019; Steinvall & Gingell, 2024a), and a magnetosonic perturbation that is launched into the downstream when the TD impinges on the shock if it has an associated pressure perturbation (Nagata et al., 2008; Maynard et al., 2007, 2008). Unlike the two minor mechanisms, we find that the dominant mechanism occurs upstream of the shock.

By tracking ions in the hybrid model (Fig. 3) and using test particle simulations (Fig. 5), we show that shock-reflected ions that cross the TD during their upstream gyration are able to gain significant additional energy from the convection electric field. Locally, this energy gain results in an acceleration efficiency of 2%, which is comparable to that of quasi-parallel shocks under steady upstream conditions(Johlander et al., 2021).

The addition of the TD results in the partition of a significant amount of energy to energetic ions ($\mathcal{E} > 10\mathcal{E}_0$), with a few ions reaching energies higher than $20\mathcal{E}_0$ (Fig. 4a and Fig. 6d). To put these numbers into perspective, for approximately Earth-like plasma conditions ($n_0 = 10$ cm^{-3}, $B_0 = 10$ nT) and with the upstream speed $v_0 = 9v_{A0}$, 10 and $20\mathcal{E}_0$ correspond to around 20 and 40 keV, respectively. It should be noted, however, that discontinuities with the large magnetic shear needed to produce significant energization ($\gtrsim 100°$) are fairly uncommon at 1 AU (Vasko et al., 2022; Y. Y. Liu et al., 2022), and that while the acceleration mechanism described in this paper may occur at the Earth's bow shock from time to time, it is not likely to be relevant for a randomly selected parcel of solar wind plasma. It is possible that this process is more important in other astrophysical contexts where highly sheared discontinuities are frequent.

5 Open Research

The simulation data and MATLAB codes used to produce the figures in this article are publicly available at (Steinvall & Gingell, 2024b).

Acknowledgments

K. Steinvall and I. Gingell are supported by the Royal Society University Research Fellowship URF\R1\191547 and associated Royal Society Enhanced Research Expenses award RF\ERE\210405. The EPOCH code used in this work was in part funded by the UK EPSRC grants EP/G054950/1, EP/G056803/1, EP/G055165/1, EP/M022463/1 and EP/P02212X/1.

References

Arber, T. D., Bennett, K., Brady, C. S., Lawrence-Douglas, A., Ramsay, M. G., Sircombe, N. J., ... Ridgers, C. P. (2015). Contemporary particle-in-cell approach to laser-plasma modelling. *Plasma Physics and Controlled Fusion*, *57*(11), 113001. doi: 10.1088/0741-3335/57/11/113001

Armstrong, T. P., Pesses, M. E., & Decker, R. B. (1985). Shock drift acceleration.

In *Collisionless shocks in the heliosphere: Reviews of current research* (p. 271-285). American Geophysical Union (AGU). doi: 10.1029/GM035p0271

Asbridge, J. R., Bame, S. J., & Strong, I. B. (1968). Outward flow of protons from the earth's bow shock. *Journal of Geophysical Research (1896-1977)*, *73*(17), 5777-5782. doi: https://doi.org/10.1029/JA073i017p05777

Blandford, R., & Eichler, D. (1987). Particle acceleration at astrophysical shocks: A theory of cosmic ray origin. *Physics Reports*, *154*(1), 1-75. doi: 10.1016/0370-1573(87)90134-7

Caprioli, D., & Spitkovsky, A. (2014, feb). Simulations of ion acceleration at non-relativistic shocks. i. acceleration efficiency. *The Astrophysical Journal*, *783*(2), 91. doi: 10.1088/0004-637X/783/2/91

Chen, L.-J., Wang, S., Wilson, L. B., Schwartz, S., Bessho, N., Moore, T., ... Avanov, L. (2018). Electron bulk acceleration and thermalization at earth's quasiperpendicular bow shock. *Phys. Rev. Lett.*, *120*, 225101. Retrieved from `https://link.aps.org/doi/10.1103/PhysRevLett.120.225101` doi: 10.1103/PhysRevLett.120.225101

Drury, L. O. (1983, aug). An introduction to the theory of diffusive shock acceleration of energetic particles in tenuous plasmas. *Reports on Progress in Physics*, *46*(8), 973. doi: 10.1088/0034-4885/46/8/002

Giacalone, J. (2003). The physics of particle acceleration by collisionless shocks. *Planetary and Space Science*, *51*(11), 659-664. (Collisionless Shocks) doi: https://doi.org/10.1016/S0032-0633(03)00101-6

Giacalone, J., Burgess, D., Schwartz, S. J., & Ellison, D. C. (1992). Hybrid simulations of protons strongly accelerated by a parallel collisionless shock. *Geophysical Research Letters*, *19*(5), 433-436. doi: 10.1029/92GL00379

Gingell, I., Schwartz, S. J., Kucharek, H., Farrugia, C. J., Fryer, L. J., Plank, J., & Trattner, K. J. (2023). Hybrid simulations of the decay of reconnected structures downstream of the bow shock. *Physics of Plasmas*, *30*(1). Retrieved from `https://doi.org/10.1063/5.0129084` (012902) doi: 10.1063/5.0129084

Hamrin, M., Gunell, H., Goncharov, O., De Spiegeleer, A., Fuselier, S., Mukherjee, J., ... Giles, B. (2019). Can reconnection be triggered as a solar wind directional discontinuity crosses the bow shock? a case of asymmetric recon-

nection. *Journal of Geophysical Research: Space Physics*, *124*(11), 8507-8523. Retrieved from `https://agupubs.onlinelibrary.wiley.com/doi/abs/10.1029/2019JA027006` doi: https://doi.org/10.1029/2019JA027006

Johlander, A., Battarbee, M., Vaivads, A., Turc, L., Pfau-Kempf, Y., Ganse, U., ... Palmroth, M. (2021, jun). Ion acceleration efficiency at the earth's bow shock: Observations and simulation results. *The Astrophysical Journal*, *914*(2), 82. doi: 10.3847/1538-4357/abfafc

Lalti, A., Khotyaintsev, Y. V., Dimmock, A. P., Johlander, A., Graham, D. B., & Olshevsky, V. (2022). A database of mms bow shock crossings compiled using machine learning. *Journal of Geophysical Research: Space Physics*, *127*(8), e2022JA030454. doi: 10.1029/2022JA030454

Lin, Y. (1997). Generation of anomalous flows near the bow shock by its interaction with interplanetary discontinuities. *Journal of Geophysical Research: Space Physics*, *102*(A11), 24265-24281. doi: 10.1029/97JA01989

Liu, T. Z., Angelopoulos, V., Vu, A., & Zhang, H. (2023). Foreshock ion motion across discontinuities: Formation of foreshock transients. *Journal of Geophysical Research: Space Physics*, *128*(4), e2022JA031161. doi: https://doi.org/10.1029/2022JA031161

Liu, T. Z., Lu, S., Angelopoulos, V., Lin, Y., & Wang, X. Y. (2018). Ion acceleration inside foreshock transients. *Journal of Geophysical Research: Space Physics*, *123*(1), 163-178. doi: https://doi.org/10.1002/2017JA024838

Liu, Y. Y., Fu, H. S., Cao, J. B., Wang, Z., He, R. J., Guo, Z. Z., ... Yu, Y. (2022, may). Magnetic discontinuities in the solar wind and magnetosheath: Magnetospheric multiscale mission (mms) observations. *The Astrophysical Journal*, *930*(1), 63. doi: 10.3847/1538-4357/ac62d2

Malkov, M. A., & Drury, L. O. (2001, apr). Nonlinear theory of diffusive acceleration of particles by shock waves. *Reports on Progress in Physics*, *64*(4), 429. doi: 10.1088/0034-4885/64/4/201

Masters, A., Stawarz, L., Fujimoto, M., Schwartz, S. J., Sergis, N., Thomsen, M. F., ... Dougherty, M. K. (2013). Electron acceleration to relativistic energies at a strong quasi-parallel shock wave. *Nature Physics*, *9*(3), 164–167. doi: 10.1038/nphys2541

Matthews, A. P. (1994). Current advance method and cyclic leapfrog for 2d mul-

tispecies hybrid plasma simulations. *Journal of Computational Physics*, *112*(1), 102-116. Retrieved from https://www.sciencedirect.com/science/article/pii/S0021999184710849 doi: https://doi.org/10.1006/jcph.1994.1084

Maynard, N. C., Burke, W. J., Ober, D. M., Farrugia, C. J., Kucharek, H., Lester, M., ... Siebert, K. D. (2007). Interaction of the bow shock with a tangential discontinuity and solar wind density decrease: Observations of predicted fast mode waves and magnetosheath merging. *Journal of Geophysical Research: Space Physics*, *112*(A12). doi: 10.1029/2007JA012293

Maynard, N. C., Farrugia, C. J., Ober, D. M., Burke, W. J., Dunlop, M., Mozer, F. S., ... Siebert, K. D. (2008). Cluster observations of fast shocks in the magnetosheath launched as a tangential discontinuity with a pressure increase crossed the bow shock. *Journal of Geophysical Research: Space Physics*, *113*(A10). doi: 10.1029/2008JA013121

Nagata, K., Hoshino, M., Jaroschek, C. H., & Takabe, H. (2008, jun). Interaction between alternating magnetic fields and a relativistic collisionless shock. *The Astrophysical Journal*, *680*(1), 627. doi: 10.1086/587640

Omidi, N., Lee, S. H., & Sibeck, D. G. (2021). Ion acceleration by foreshock bubbles. *Journal of Geophysical Research: Space Physics*, *126*(5), e2020JA028924. doi: https://doi.org/10.1029/2020JA028924

Pesses, M. E., Decker, R. B., & Armstrong, T. P. (1982). The acceleration of charged particles in interplanetary shock waves. *Space Science Reviews*, *32*(1), 185–204. Retrieved from https://doi.org/10.1007/BF00225184 doi: 10.1007/BF00225184

Schwartz, S. J., Paschmann, G., Sckopke, N., Bauer, T. M., Dunlop, M., Fazakerley, A. N., & Thomsen, M. F. (2000). Conditions for the formation of hot flow anomalies at earth's bow shock. *Journal of Geophysical Research: Space Physics*, *105*(A6), 12639-12650. doi: https://doi.org/10.1029/1999JA000320

Steinvall, K., & Gingell, I. (2024a). The influence of rotational discontinuities on the formation of reconnected structures at collisionless shocks—hybrid simulations. *Journal of Geophysical Research: Space Physics*, *129*(1), e2023JA032101. doi: https://doi.org/10.1029/2023JA032101

Steinvall, K., & Gingell, I. (2024b, February). *Simulation data archive: Enhanced*

ion acceleration due to high-shear tangential discontinuities upstream of quasi-perpendicular shocks [Dataset]. Zenodo. Retrieved from https://doi.org/10.5281/zenodo.10629193 doi: 10.5281/zenodo.10629193

Turner, D. L., Wilson, L. B., Liu, T. Z., Cohen, I. J., Schwartz, S. J., Osmane, A., ... Burch, J. L. (2018, September). Autogenous and efficient acceleration of energetic ions upstream of Earth's bow shock. *Nature*, *561*(7722), 206–210. doi: 10.1038/s41586-018-0472-9

Vasko, I. Y., Alimov, K., Phan, T., Bale, S. D., Mozer, F. S., & Artemyev, A. V. (2022, feb). Kinetic-scale current sheets in the solar wind at 1 au: Scale-dependent properties and critical current density. *The Astrophysical Journal Letters*, *926*(2), L19. Retrieved from https://dx.doi.org/10.3847/2041-8213/ac4fc4 doi: 10.3847/2041-8213/ac4fc4

Wilson, L. B., Chen, L.-J., & Roytershteyn, V. (2021). The discrepancy between simulation and observation of electric fields in collisionless shocks. *Frontiers in Astronomy and Space Sciences*, *7*. Retrieved from https://www.frontiersin.org/articles/10.3389/fspas.2020.592634 doi: 10.3389/fspas.2020.592634

Zhang, H., Zong, Q., Connor, H., Delamere, P., Facskó, G., Han, D., ... Yao, S. (2022). Dayside Transient Phenomena and Their Impact on the Magnetosphere and Ionosphere. *Space Science Reviews*, *218*(5), 40. doi: 10.1007/s11214-021-00865-0